Geochemical Perspectives Letters

Abiotic syntheses of pyrite: clues to assess the biogenicity of pyrite spherules

C. Truong[1,#*], S. Bernard[1], A. Gorlas[2], F. Guyot[1,3]

OPEN ACCESS

https://doi.org/10.7185/geochemlet.2438

Abstract

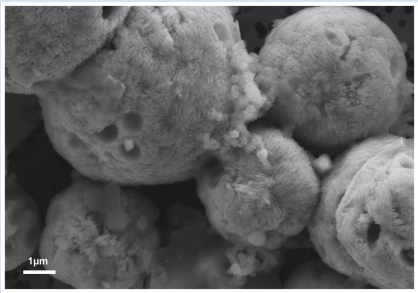

Life proliferates almost everywhere on Earth but determining whether or not hyperthermophile microorganisms have colonised a given hydrothermal environment, such as black smoker chimneys, remains challenging. Some mineral phases like pyrite spherules have been proposed to possibly serve as biosignatures. Yet, little is known about the specificities of pyrites produced *via* abiotic processes under hydrothermal conditions, making these pyrite spherules only potential biosignatures at best. Here, we report results of abiotic syntheses of pyrites under conditions reproducing those existing in the chimneys of black smokers, in the presence or in the absence of various organic compounds. We experimentally show that no pyrite is produced in the absence of organic material, whereas the chemical nature of the organic compounds controls the shape and crystallinity of the pyrite produced. The presence of complex organic matter, here compounds derived from lysed cells, appears necessary for the production of pyrite spherules previously described as biogenic, suggesting that the pyrite spherules detected in natural black smokers may not be considered as biogenic *stricto sensu*, but rather as proxies of the presence of microorganisms.

Received 18 April 2024 | Accepted 17 July 2024 | Published 1 October 2024

Letter

In 50 years of research, the known thermal limit of life has been extended several times, rising from 70 °C, to over 100 °C, to 113 °C and finally to 122 °C (Brock and Freeze, 1969; Blöch *et al.*, 1997; Kashefi and Lovley, 2003; Takai *et al.*, 2008). Current estimates set the maximum temperature at which life could exist between 113 °C and 150 °C (Stetter, 1999; Cowan and Tow, 2004; Merino *et al.*, 2019). Life could therefore withstand the temperature conditions inside the external parts of chimneys of black smokers, whose pore spaces could harbour microhabitats for hyperthermophilic microorganisms.

The incubation of chimney pieces enables the isolation of various microbial strains (*e.g.*, Takai *et al.*, 2001; Nercessian *et al.*, 2003). The detection of biomarkers in chimney samples, such as the gene coding for 16S ribosomal RNA (Schrenk *et al.*, 2003) or bacterial and archaeal lipids (Blumenberg, 2007), has led some authors to suggest that chimneys are, or have been, colonised by (hyper)thermophilic microorganisms. However, biomarkers may have been transported from the surrounding fluids within the chimney wall after their production. To date, there is still no direct observation of the presence of (hyper)thermophilic microorganisms in the walls of black smoker chimneys. The abrupt fluctuations in temperature, pH and redox conditions of sulfur-rich hydrothermal vents (Tivey *et al.*, 2002; Schrenk *et al.*, 2003; Lin *et al.*, 2016) make *in situ* observations difficult.

A recent study of chimney samples from a black smoker at the Trans-Atlantic Geotraverse (TAG) site on the Mid-Atlantic Ridge revealed the presence of pyrite (FeS_2) spherules, whose morphologies and chemical characteristics suggested that they constitute a biosignature (Truong *et al.*, 2024). These polycrystalline pyrite spherules exhibit a rounded shape, with a diameter ranging between 2 µm and 100 µm (Fig. 1 and Fig. 2a) showing some similarities with pyrite spherules made in mineralised cultures of the hyperthermophilic *Thermococcus kodakarensis* KOD1 archaeon (Truong *et al.*, 2023) and with pyrite spherules found in culture experiments at ambient temperature (Berg *et al.*, 2020; Duverger *et al.*, 2020). Moreover, these pyrite spherules contain organic compounds displaying a spectroscopic signature similar to that of a living cell, with a predominance of amide groups (Fig. 1). The similarities between the pyrite spherules produced in the presence of *Thermococcales* and those observed in the chimneys at the TAG site now call for a better understanding of pyrite production, the possible abiotic production of such pyrite spherules needs to be excluded to consider them biosignatures. In other words, a number of questions remain to be addressed. Can pyrite spherules be produced abiotically? Is organic matter necessary for their production? Does the nature of organic material present influence the morphology and microtexture of these spherules? Do the pyrites record information from the initially present organic matter? Providing answers to these questions requires conducting abiotic syntheses of pyrites

1. Institut de Minéralogie, de Physique des Matériaux et de Cosmochimie (IMPMC), Sorbonne Université- Museum National d'Histoire Naturelle, CNRS, Paris, France
2. Institute for Integrative Biology of the Cell (I2BC), Université Paris-Saclay, CEA, CNRS, Gif-sur-Yvette, France
3. Institut Universitaire de France (IUF), Paris, France
Current address: Institut de Microbiologie de la Méditerranée (IMM), CNRS, Aix-Marseille Université (AMU), Marseille, France
* Corresponding author (email: ctruong@imm.cnrs.fr)

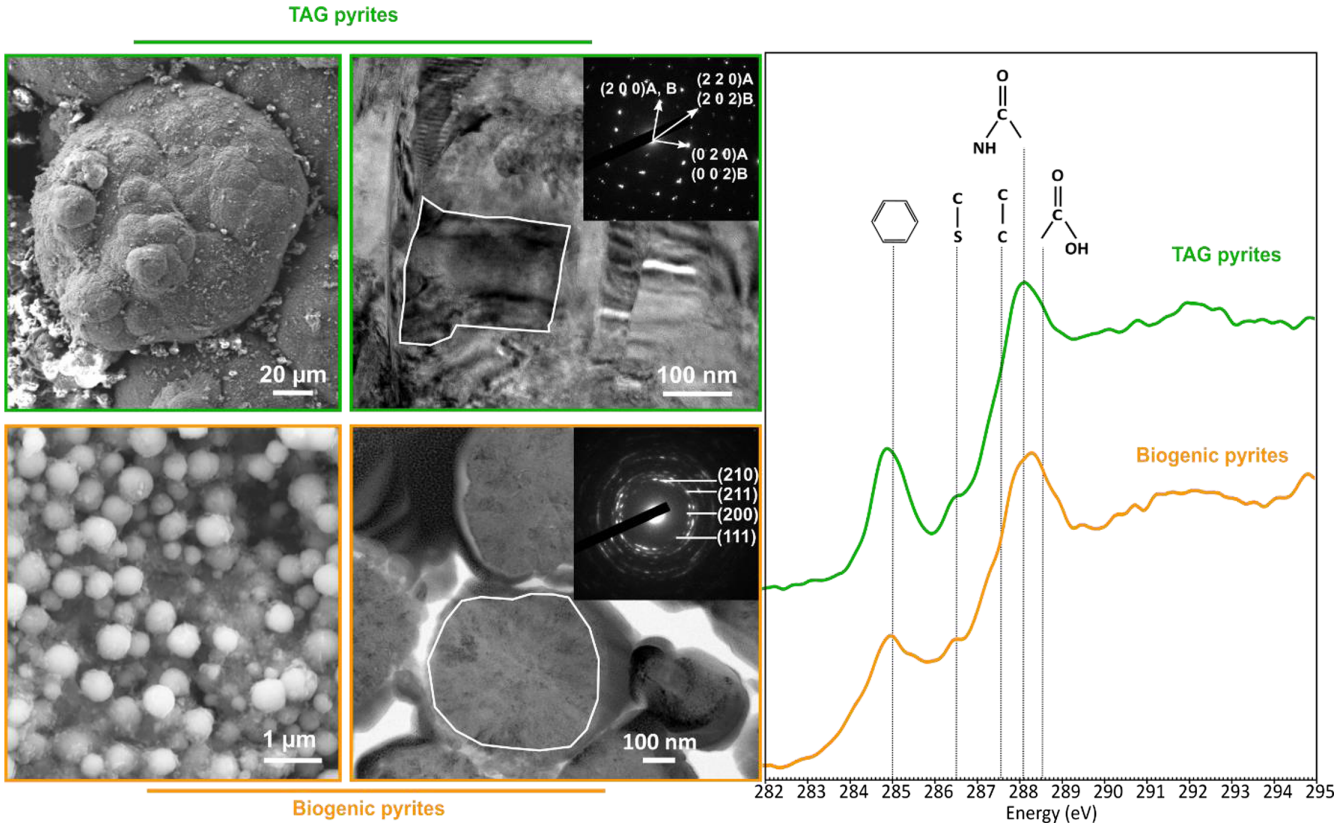

Figure 1 SEM, TEM (left) and STXM characterisation (right) of pyrite aggregates isolated from TAG hydrothermal field (in green) compared to biogenic pyrites produced by living *T. kodakarensis* KOD1 cells (in orange) (Truong *et al.*, 2023).

under conditions mimicking those existing within chimneys of black smokers.

Here, we report the results of abiotic syntheses carried out under experimental conditions reproducing those of black smokers., *i.e.* in a medium rich in reactive Fe^{2+} and reduced sulfur compounds (Gartman *et al.*, 2011; Findlay *et al.*, 2016). Solutions containing colloidal sulfur (20 mM), ferrous iron Fe^{2+} ($FeSO_4$ 5 mM) and sulfide (Na_2S 1.3 mM) were submitted to 85 °C for 96 hr in the presence (or not) of various carbon compounds (Table 1). First, a control experiment was carried out in the absence of any organic material. Then, a series of two syntheses were conducted in the presence of organic compounds unrelated to archaea cells: (1) in the presence of poorly soluble and poorly reactive graphitic carbon flakes, and (2) in the presence of the yeast extract and tryptone often used for the growth of cultures of *Thermococcales* (*e.g.*, Gorlas *et al.*, 2015, 2018, 2022). Another series of three syntheses were also conducted in the presence of organic compounds produced by hyperthermophilic *T. kodakarensis* KOD1 cells: (1) in the presence of cell envelopes consisting of lipid-rich cell membranes and S-layer proteins, recovered from cell lysis, named hereafter KOD1 envelopes, (2) in the presence of the supernatant and intracellular material, the last being recovered from cell lysis, hereafter named KOD1 supernatant + intracellular material, and (3) in the presence of whole cell lysates, *i.e.* containing the envelopes and the intracellular material of KOD1, hereafter named KOD1 lysates (for each fraction, see experimental protocol in Supplementary Information). The products of these syntheses were then characterised using scanning electron microscopy (SEM), transmission electron microscopy (TEM) and scanning transmission X-ray microscopy coupled to X-ray absorption near edge structure spectroscopy (STXM-XANES) to document the nature, the morphology and the microtexture of the pyrite produced as well as the nature of their potential organic content.

No pyrite was produced in the absence of organic material (Fig. 2c), highlighting that the presence of colloidal sulfur, ferrous iron and sulfide is not sufficient to produce pyrite under the experimental conditions chosen in this study. Indeed, it is known that higher concentrations of sulfides (typically 180 mM of Na_2S instead of the 1.3 mM used in the present study) are needed to allow the H_2S pathway of abiotic pyrite precipitation (*e.g.*, Mansor and Fantle, 2019). On the other hand, pyrites were produced in almost all the syntheses conducted in the presence of organic matter, with sizes, morphologies and microtextures depending on the organic matter used for synthesis. Pyrites produced in the presence of graphitic carbon flakes are submicrometric (around 1 µm or less) and can be observed on the surface of graphitic carbon flakes as sand-rose-like crystals (Fig. 2e,f). Similarly, the pyrites produced in the presence of yeast extract and tryptone display a sand-rose shape, but measure 2 to 10 µm in diameter (Fig. 2d). In the presence of KOD1 envelopes, pyrites appear as spherules measuring 10 µm in diameter, with no crystallites visible at the SEM scale (Fig. 2h). This is in contrast to the pyrite spherules measuring 2 to 5 µm produced in the presence of KOD1 lysates (Fig. 2i). Of note, no pyrite was produced in the presence of KOD1 intracellular material only (Fig. 2j). One explanation could be the need for reactive surface areas available for pyrite nucleation and growth, which are absent without organic matter and possibly insufficient in the synthesis with KOD1 intracellular matter alone. As yeast extract and tryptone also are very soluble organic compounds, another explanation could involve the concentration of soluble organic matter which has been demonstrated to influence organomineralisation (Cosmidis *et al.*, 2019).

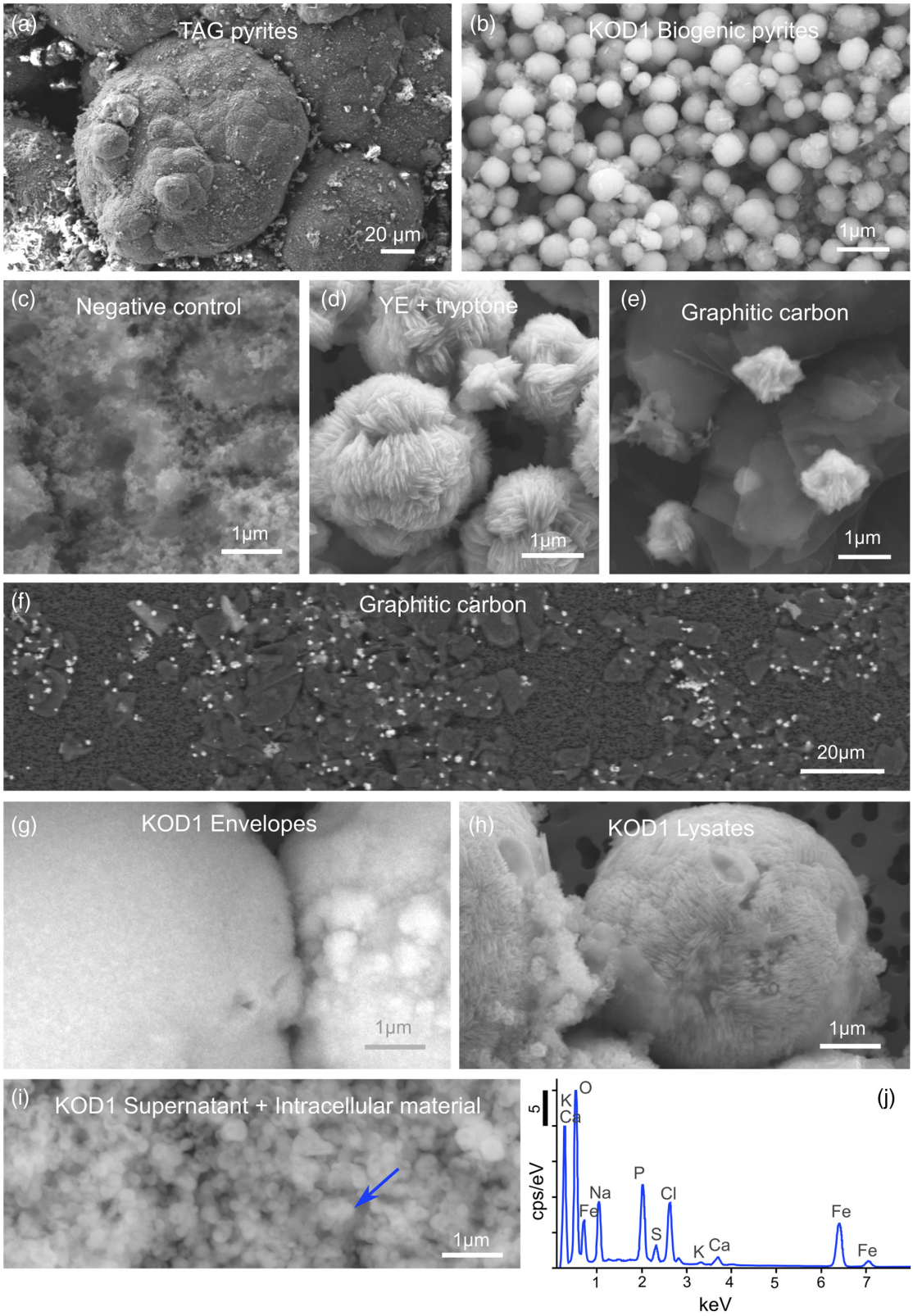

Figure 2 SEM investigations of pyrites produced at 85 °C for 96 hr in a colloidal sulfur and Fe2+-rich medium compared to **(a)** pyrites isolated from TAG hydrothermal field, and **(b)** biogenic pyrite spherules produced in presence of KOD1 cells (Truong *et al.*, 2023). **(c)** No pyrite produced in absence of organic matter. **(d)** Pyrites produced in presence of yeast extract and tryptone. **(e–f)** Micrometric pyrite crystals produced in presence of graphitic carbon. **(g)** Massive rounded pyrites measuring 10 µm produced in presence of KOD1 envelopes. **(h)** Rounded pyrites produced in presence of KOD1 lysates. **(i)** No pyrite produced in presence of both KOD1 supernatant and intracellular material but a predominance of colloidal phosphates as evidence by **(j)** associated EDXS spectrum.

Table 1 Summary of the production of pyrites and their carbon content for abiotic synthesis made with different types of organic matter (85 °C – 96 hr), compared to biogenic pyrites (*i.e.* KOD1) and TAG pyrites.

Samples	TAG	KOD1	KOD1 Lysates	KOD1 Envelopes	KOD1 Intracellular material	YE + tryptone	Graphite	Negative control
Organic matter	Unkown	KOD1 5.10^7 cells/mL^{-1}	- KOD1 lysates (100 mL at 5.10^7 cells/mL^{-1})	- KOD1 envelopes (100 mL at 5.10^7 cells/mL^{-1})	- KOD1 supernatants and intracellular material (100 mL at 5.10^7 cells/mL^{-1})	- Yeast extract 1g/L - Tryptone 1g/L	Graphitic carbon 2g/L	None
Pyrite	Yes	Yes	Yes	Yes	No	Yes	Yes	No
$[C]_{STXM}$	3.58	4.65	4.45	2.12	na	1.86	2.08	na

Overall, considering the sizes and morphologies at the micrometre scale, only pyrites produced in the presence of KOD1 envelopes or KOD1 lysates show similarities with pyrite spherules produced in the presence of living *T. kodakarensis* KOD1 (Truong *et al.*, 2023) and with pyrite spherules reported in the chimney walls of black smokers (Truong *et al.*, 2024).

In line with previous observations, TEM and STXM analyses revealed that pyrites produced in the presence of graphitic carbon flakes exhibit significant differences from spherules produced in the presence of *T. kodakarensis* cells. The crystallographic domains are between 200 and 300 nm in size, and the low $[C]_{STXM}$ value of 2.08 suggests that these pyrites associated with graphite have trapped a very small amount of carbon, preventing a proper XANES spectrum to be collected (Fig. 3, Table 1). Pyrites produced in the presence of yeast extract and tryptone also display specific characteristics: they have crystallographic domains of several hundred nanometres and have trapped only a small amount of carbon, as evidenced by a very low $[C]_{STXM}$ value of 1.86. The XANES spectrum of this organic material is dominated by an absorption feature at 288.6 eV (attributed to COOH groups; Le Guillou *et al.*, 2018) (Fig. 3). Finally, pyrites produced in the presence of KOD1 envelopes do not display chemical characteristics similar to those of pyrite spherules produced in the presence of living cells: the microtexture itself is not very different, with crystalline domains between 50 and 100 nm in size, but they contain less organic matter (the $[C]_{STXM}$ value is only 2.12). The XANES spectrum of this organic carbon is consistent with lipids, with a small absorption feature at 285.1 eV (attributed to C=C bonds; Le Guillou *et al.*, 2018) and a main absorption feature at 287.6 eV (attributed to C-H bonds; Le Guillou *et al.*, 2018) (Fig. 3).

In contrast, the pyrite spherules produced in the presence of KOD1 lysates closely resemble the pyrite spherules produced in the presence of living *T. kodakarensis* cells: the microtexture is identical with crystalline domains smaller than 10 nm, and the carbon content is similar, with a $[C]_{STXM}$ value of 4.45. The XANES spectrum of this organic material shows similar features to the spectra of living cells (Benzerara *et al.*, 2006; Miot *et al.*, 2009; Li *et al.*, 2014; Picard *et al.*, 2021; Truong *et al.*, 2023) and to the spectrum of organic material trapped within the pyrite spherules produced in the presence of living *T. kodakarensis* cells (Truong *et al.*, 2023), with absorption features at 285.1, 286.5, 287.6, 288.1 and 288.6 eV, attributed to C=C bonds, C-S bonds, C-H bonds, amide groups and carboxylic groups, respectively (Le Guillou *et al.*, 2018) (Fig. 3). Indeed, these pyrites can be considered to have been produced according to the same recipe (with the same ingredients) as the pyrite spherules produced in the presence of living *T. kodakarensis cells*, the only difference being that here the cells were dead.

Altogether, the results of these syntheses strongly suggest that the chemical nature of the initial organic matter controls the final morphology, microtexture and organic content of the pyrite produced. They also evidence that the production of pyrite spherules is – except for the spherule size distribution – not controlled by live *T. kodakarensis* cells but that it is rather a production induced by their biomass. An explanation for the production of pyrite spherules may reside in the highly reactive surfaces of microbial cells, either living or dead. Microbial surfaces exhibit organic ligands, which are indeed characterised by a net negative charge, thus conferring upon them the capability of creating strong bonds with Fe^{2+} (Beveridge, 1989). Nevertheless, it cannot be ruled out that complex negatively charged abiotic compounds may also play this role. Another important factor may be that organic matter acts as a redox-active component that can promote the formation of intermediate sulfur species, *i.e.* polysulfides. The presence or enrichment of certain functional groups can have a direct impact on sulfide production, notably *via* the presence of surface oxygen groups.

The amount of carbon sequestered inside pyrite spherules appears to be important for their potential use as biosignatures. In a recent experimental study, Nabeh *et al.* (2022) investigated the precipitation of iron sulfides in the presence of various organic compounds (amino acids, tryptone, yeast extract and microbial cells). Their results demonstrated, consistent with the present results, that the sequestration of organic material by iron sulfides in the presence of amino acids, tryptone and yeast extract is low compared to the sequestration of organic material by iron sulfides in the presence of microbial cells (Nabeh *et al.*, 2022). Their explanation involved the binding of iron sulfides and organic molecules on the surface of cells and the formation of organo-mineral aggregates (Nabeh *et al.*, 2022). According to the present results, another important factor would be, in addition to surface availability, the solubility of the organic material present and (maybe most importantly), its oxido-reduction potential. On the one hand, organic compounds locally control sulfide saturation conditions *via* their redox potential, which influences the size of the crystalline domains (Nývlt, 1968). On the other hand, if very soluble, they may be sequestrated within the pyrites at the grain sub-joints, thus stabilising the ultra-small domains and protecting them from recrystallisation.

Regarding the size range, the pyrite spherules found within the chimney walls of TAG mound's black smoker (Fig. 1) (Truong *et al.*, 2024) are more similar to the pyrite spherules produced in the presence of KOD1 lysates than to the pyrites produced in the presence of living *T. kodakarensis* cells. Still, the pyrite spherules from the TAG mound display a larger variability in size and larger crystallographic domains (~200 nm; Figs. 1 and 3). Growth and/or coalescence of pre-existing

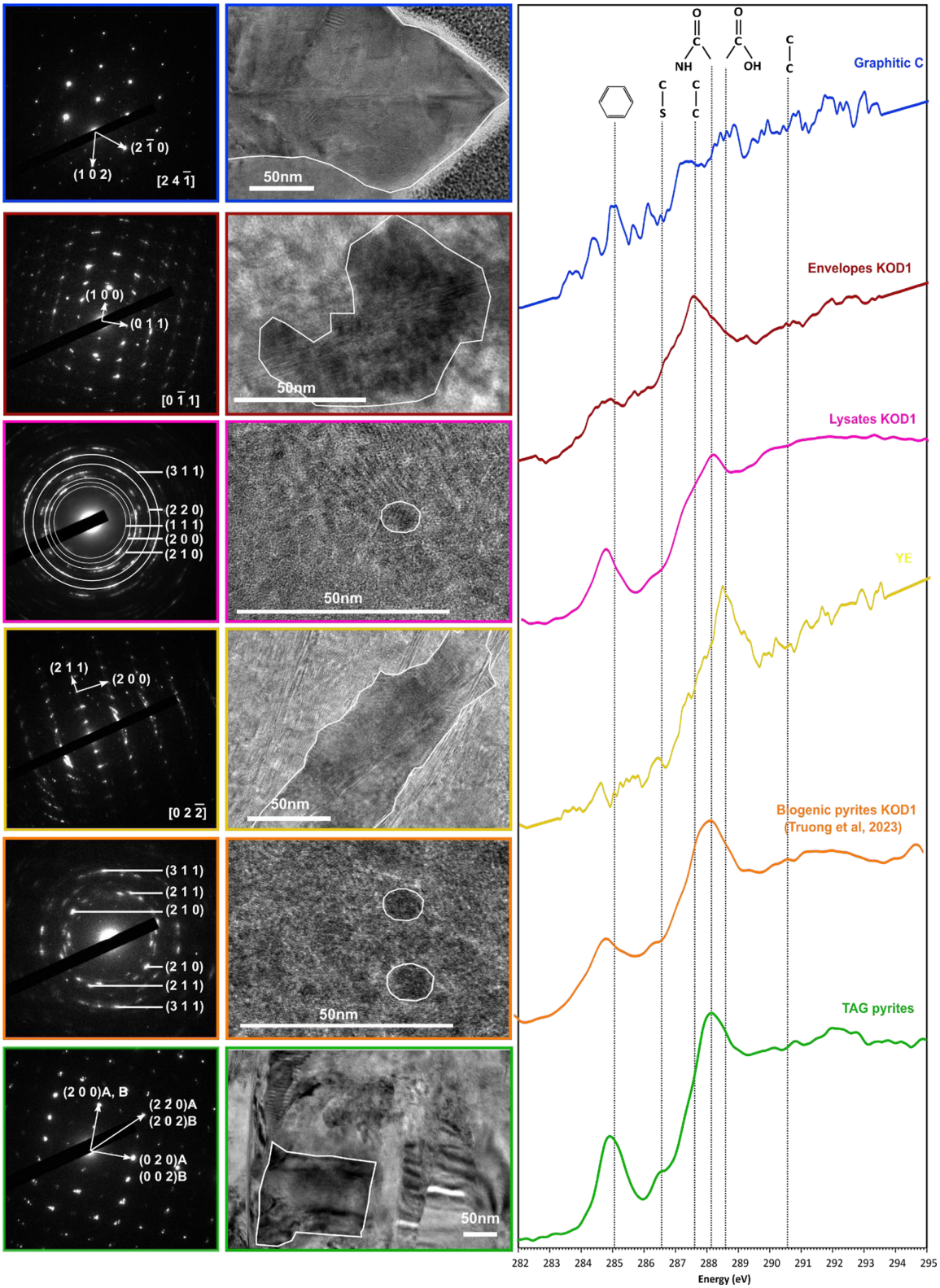

Figure 3 TEM, associated SAED patterns and STXM characterisation of TAG rounded pyrites (in green), biogenic pyrites (in orange) and abiotic counterparts produced at 85 °C for 96 hr in a colloidal sulfur and Fe^{2+}-rich medium: yeast extract and tryptone (in yellow), KOD1 lysates (in pink), KOD1 envelopes (in red) and graphitic carbon (in blue). Of note, spots (100) and (011) are not allowed by the Pa3 space group of pyrite but are here enabled by double diffraction. The white outines correspond to the crystalline domain diffracted in the associated SAED pattern (TAG pyrites; YE; envelopes KOD1; Graphitic C), or to a putative crystalline domain for powder SAED pattern (biogenic pyrite KOD1; lysates KOD1).

spherules as well as the constant, or at least unlimited and non-limiting, supply of Fe and S in natural hydrothermal environments for a duration obviously longer than the duration of the present syntheses may explain bigger sizes in the natural environment. Other parameters need to be better mimicked, especially the pressure and temperature conditions: pressure

conditions are higher at the TAG mound (located at a depth of 3650 m, *i.e.* a hydrostatic pressure of 35 MPa) and temperatures may vary to values significantly higher than 85 °C, eventually leading to the recrystallisation and growth of pyrite produced at lower temperature. There is no doubt that additional abiotic syntheses as well as experimental fossilisation of biogenic pyrite spherules should be conducted to further investigate the possibility of unambiguously determining the origin (*i.e.* biogenic or abiotic) of natural pyrite spherules.

A trail to follow could be the molecular structure of the organic material trapped within the pyrites. As demonstrated here, the chemical nature of the organic material detected within the pyrite spherules may inform the nature of organic compounds initially present in the system. Yet, hydrothermal vents are the location of extensive mixing between seawater (possibly rich in biogenic organic materials) and hydrothermal fluids (possibly rich in abiotic organic materials) (*e.g.*, Maruyama *et al.*, 1993; Dick *et al.*, 2010), making it difficult to identify sources. Organic compounds can be transported, allowing their presence within walls of chimney even though they have not been produced there. In such a case, one could expect some chemical selection (different organic compounds may not be transported similarly), which does not seem to be the case according to XANES data (Truong *et al.*, 2024). Given the thermal maturation that such mineral structures have inevitably experienced, it remains difficult to expect to detect pristine biogenic organic materials: amino acids are for instance irreversibly destroyed above 240 °C (Bada *et al.*, 1995), which is a temperature well below that of the hydrothermal fluid circulating through a chimney (*e.g.*. Tivey *et al.*, 2002).

All in all, can we consider the pyrite spherules as biosignatures? By definition, a biosignature provides irrefutable proof of biogenicity. The conformity of a biosignature does not only depend on its production by living organisms, but also on the inability of abiotic processes to produce it. There are no irrefutable criteria on which to base the claim that a mineral is biogenic: mineral biosignatures may thus not exist as such. To move forward, we need to rethink the concept of biosignature in terms of probability rather than irrefutability (McMahon and Jordan, 2022; Malaterre *et al.*, 2023). Given the environmental conditions, the morphology, microtexture and organic content (both its value and its nature), is it more likely that the mineral structure investigated was produced by (or in the presence of) living microorganisms or by abiotic processes? Here, the production of pyrite spherules involves the presence of ferrous iron, reactive sulfur in the form of colloidal sulfur as well as the presence of reactive surface and soluble cellular organic material. Within hydrothermal vents, colloidal sulfur can be produced by both living microorganisms and by abiotic processes (*e.g.*, Findlay, 2016). In contrast, cellular organic material is exclusively produced by living organisms, or at least, a mixture of organic molecules similar in composition to a mixture that life produces is likely to have been produced by life.

In such a scheme, it could be concluded that it is more likely that living organisms were involved in the production of the pyrite spherules from the TAG site given their size, morphology, microtexture and organic content (both its quantity and nature). However, an abiotic production of similar pyrite spherules in the presence of abiotic macromolecular organic molecules cannot be ruled out at this stage without further experimental research, using complex abiotic organic molecules while deploying additional characterisation (including isotopic measurements). Plus, given that temperature and/or supersaturation may influence pyrite production, experiments exploring the influence of both temperature and hydrodynamic conditions remain to be conducted.

Author Contributions

CT, SB, AG and FG contributed to the conception and design of the study. AG and CT conducted the *Thermococcales* cultures and the preparation of the lysates. CT conducted the mineralisation process in anoxic conditions. FG and CT conducted the electron microscopy analyses. SB and CT conducted the STXM analyses. CT wrote the first draft of the manuscript. CT, SB, AG and FG wrote the sections of the manuscript. All authors contributed to the manuscript revision, read, and approved the submitted version.

Acknowledgements

We acknowledge the support of the support of the Bicose 2 campaign (IFREMER), IMPMC-MNHN microscopy platform and of the SOLEIL HERMES beamline. We thank Erwan Roussel and Marie-Anne Cambon-Bonavita (IFREMER) for providing us the valuable samples from the Bicose 2 campaign, Elisabeth Malassis (IMPMC) for her administrative support, Sylvain Pont (IMPMC) for his help in SEM-EDXS, Jean-Michel Guigner (IMPMC) for his help in TEM, David Troadec (IEMN) for the preparation of the FIB sections, Corentin Le Guillou (UMET) for his help with STXM and Stefan Stanescu for his expert support of HERMES beamline at SOLEIL. AG was supported by the Agence Nationale de la Recherche, project HYPERBIOMIN (ANR-20-CE02-0001-01). FG was supported by Institut Universitaire de France.

Editor: Andreas Kappler

Additional Information

Supplementary Information accompanies this letter at https://www.geochemicalperspectivesletters.org/article2438.

Cite this letter as: Truong, C., Bernard, S., Gorlas, A., Guyot, F. (2024) Abiotic syntheses of pyrite: clues to assess the biogenicity of pyrite spherules. *Geochem. Persp. Let.* 32, 27–33. https://doi.org/10.7185/geochemlet.2438

References

Bada, J.L., Miller, S.L., Zhao, M. (1995) The stability of amino acids at submarine hydrothermal vent temperatures. *Origins of Life and Evolution of the Biosphere* 25, 111–118. https://doi.org/10.1007/BF01581577

Berg, J.S., Duverger, A., Cordier, L., Laberty-Robert, C., Guyot, F., Miot, J. (2020) Rapid pyritization in the presence of a sulfur/sulfate-reducing bacterial consortium. *Scientific Reports* 10, 8264. https://doi.org/10.1038/s41598-020-64990-6

Benzerara, K., Menguy, N., López-García, P., Brown, G. Jr. (2006) Nanoscale detection of organic signatures in carbonate microbialites. *Proceedings of the National Academy of Sciences* 103, 9440–9445. https://doi.org/10.1073/pnas.0603255103

Beveridge, T. J. (1989) Role of Cellular Design in Bacterial Metal Accumulation and Mineralization. *Annual Review of Microbiology* 43, 147–171. https://doi.org/10.1146/annurev.mi.43.100189.001051

Blöchl, E., Rachel, R., Burggraf, S., Hafenbradl, D., Jannasch, H.W., Stetter, K.O. (1997) *Pyrolobus fumarii*, gen. and sp. nov., represents a novel group of archaea, extending the upper temperature limit for life to 113°C. *Extremophiles* 1, 14–21. https://doi.org/10.1007/s007920050010

Blumenberg, M., Seifert, R., Petersen, S., Michaelis, W. (2007) Biosignatures present in a hydrothermal massive sulfide from the Mid-Atlantic Ridge. *Geobiology* 5, 435–450. https://doi.org/10.1111/j.1472-4669.2007.00126.x

Brock, T.D., Freeze, H. (1969) *Thermus aquaticus* gen. n. and sp. n., a nonsporulating extreme thermophile. *Journal of Bacteriology* 98, 289–297. https://doi.org/10.1128/jb.98.1.289-297.1969

Cosmidis, J., Nims, C.W., Diercks, D., Templeton, A.S. (2019) Formation and stabilization of elemental sulfur through organomineralization. *Geochimica et Cosmochimica Acta* 247, 59–82. https://doi.org/10.1016/j.gca.2018.12.025

Cowan, D.A., Tow, L.A. (2004) Endangered Antarctic environments. *Annual Reviews in Microbiology* 58, 649–690. https://doi.org/10.1146/annurev.micro.57.030502.090811

Dick, G.J., Tebo, B.M. (2010) Microbial diversity and biogeochemistry of the Guaymas Basin deep-sea hydrothermal plume. *Environmental Microbiology* 12, 1334–1347. https://doi.org/10.1111/j.1462-2920.2010.02177.x

Duverger, A., Berg, J.S., Busigny, V., Guyot, F., Bernard, S., Miot, J. (2020) Mechanisms of pyrite formation promoted by sulfate-reducing bacteria in pure culture. *Frontiers in Earth Science* 8, 588310. https://doi.org/10.3389/feart.2020.588310

Gartman, A., Yücel, M., Madison, A., Chu, D., Ma, S., Janzen, C., Becker, E., Beinart, R., Girguis, P., Luther, G. (2011) Sulfide oxidation across diffuse flow zones of hydrothermal vents. *Aquatic Geochemistry* 17, 583–601. https://doi.org/10.1007/s10498-011-9136-1

Gorlas, A., Marguet, E., Gill, S., Geslin, C., Guigner, J.-M., Guyot, F., Forterre, P. (2015) Sulfur vesicles from Thermococcales: A possible role in sulfur detoxifying mechanisms. *Biochimie* 118, 356–364. https://doi.org/10.1016/j.biochi.2015.07.026

Gorlas, A., Jacquemot, P., Guigner, J.-M., Gill, S., Forterre, P., Guyot, F. (2018) Greigite nanocrystals produced by hyperthermophilic archaea of Thermococcales order. *PLoS One* 13, e0201549. https://doi.org/10.1371/journal.pone.0201549

Gorlas, A., Mariotte, T., Morey, L., Truong, C., Bernard, S., Guigner, J.-M., Oberto, J., Baudin, F., Landrot, G., Baya, C., Le Pape, P., Morin, G., Forterre, P., Guyot, F. (2022) Precipitation of greigite and pyrite induced by Thermococcales: an advantage to live in Fe- and S-rich environments? *Environmental Microbiology* 24, 626–642. https://doi.org/10.1111/1462-2920.15915

Findlay, A.J. (2016) Microbial impact on polysulfide dynamics in the environment. *FEMS Microbiology Letters* 363, fnw103. https://doi.org/10.1093/femsle/fnw103

Kashefi, K., Lovley, D.R. (2003) Extending the upper temperature limit for life. *Science* 301, 934–934. https://doi.org/10.1126/science.1086823

Le Guillou, C., Bernard, S., De la Peña, F., Le Brech, Y. (2018) XANES-Based Quantification of Carbon Functional Group Concentrations. *Analytical Chemistry* 90, 8379–8386. https://doi.org/10.1021/acs.analchem.8b00689

Li, J.H., Bernard, S., Benzerara, K., Beyssac, O., Allard, T., Cosmidis, J., Moussou, J. (2014) Impact of biomineralization on the preservation of microorganisms during fossilization: An experimental perspective. *Earth and Planetary Science Letters* 400, 113–122. https://doi.org/10.1016/j.epsl.2014.05.031

Lin, T., Ver Eecke, H., Breves, E., Dyar, M., Jamieson, J., Hannington, M., Dahle, H., Bishop, J., Lane, M., Butterfield, D., Kelley, D., Lilley, M., Baross, J., Holden, J. (2016) Linkages between mineralogy, fluid chemistry, and microbial communities within hydrothermal chimneys from the Endeavour segment, Juan de Fuca ridge. *Geochemistry Geophysics Geosystems* 17, 300–323. https://doi.org/10.1002/2015GC006091

Malaterre, C., Ten Kate, I.L., Baqué, M., Debaille, V., Grenfell, J.L., Javaux, E.J., Klenner, F., Lara, Y.J., McMahon, S., Moore, K., Noack, L., Patty L., Postberg, F. (2023) Is there such a thing as a biosignature? *Astrobiology* 23, 1213–1227. https://doi.org/10.1089/ast.2023.0042

Mansor, M., Fantle, M.S. (2019) A novel framework for interpreting pyrite-based Fe isotope records of the past. *Geochimica et Cosmochimica Acta* 253, 39–62. https://doi.org/10.1016/j.gca.2019.03.017

Maruyama, A., Mita, N., Higashihara, T. (1993) Particulate materials and microbial assemblages around the Izena black smoking vent in the Okinawa Trough. *Journal of Oceanography* 49, 353–367. https://doi.org/10.1007/BF02269570

McMahon, S., Jordan, S.F. (2022) A fundamental limit to the search for the oldest fossils. *Nature Ecology & Evolution* 6, 832–834. https://doi.org/10.1038/s41559-022-01777-0

Merino, N., Aronson, H.S., Bojanova, D.P., Feyhl-Buska, J., Wong, M.L., Zhang, S., Giovannelli, D. (2019) Living at the extremes: extremophiles and the limits of life in a planetary context. *Frontiers in Microbiology* 10, 780. https://doi.org/10.3389/fmicb.2019.00780

Miot, J., Benzerara, K., Obst, M., Kappler, A., Hegler, F., Schädler, S., Bouchez, C., Guyot, F., Morin, G. (2009) Extracellular iron biomineralization by photoautotrophic iron-oxidizing bacteria. *Applied Environmental Microbiology* 75, 5586–5591. https://doi.org/10.1128/AEM.00490-09

Nabeh, N., Brokaw, C., Picard, A. (2022) Quantification of Organic Carbon Sequestered by Biogenic Iron Sulfide Minerals in Long-Term Anoxic Laboratory Incubations. *Frontiers in Microbiology* 13, 662219. https://doi.org/10.3389/fmicb.2022.662219

Nercessian, O., Reysenbach, A.L., Prieur, D., Jeanthon, C. (2003) Archaeal diversity associated with in situ samplers deployed on hydrothermal vents on the East Pacific Rise (13°N). *Environmental Microbiology* 5, 492–502. https://doi.org/10.1046/j.1462-2920.2003.00437.x

Nývlt, J. (1968) Kinetics of nucleation in solutions. *Journal of Crystal Growth* 3, 377–383. https://doi.org/10.1016/0022-0248(68)90179-6

Picard, A., Gartman, A., Girguis, P.R. (2021) Interactions Between Iron Sulfide Minerals and Organic Carbon: Implications for Biosignature Preservation and Detection. *Astrobiology* 21, 587–604. https://doi.org/10.1089/ast.2020.2276

Schrenk, M., Kelley, D., Delaney, J., Baross, J. (2003) Incidence and diversity of microorganisms within the walls of an active deep-sea sulfide chimney. *Applied and Environmental Microbiology* 69, 3580–3592. https://doi.org/10.1128/AEM.69.6.3580-3592.2003

Stetter, K.O. (1999) Extremophiles and their adaptation to hot environments. *FEBS Letters* 452, 22–25. https://doi.org/10.1016/S0014-5793(99)00663-8

Takai, K., Komatsu, T., Inagaki, F., Horikoshi, K. (2001) Distribution of Archaea in a black smoker chimney structure. *Applied Environmental Microbiology* 67, 3618–3629. https://doi.org/10.1128/AEM.67.8.3618-3629.2001

Takai, K., Nakamura, K., Toki, T., Tsunogai, U., Miyazaki, M., Miyazaki, J., Horikoshi, K. (2008) Cell proliferation at 122°C and isotopically heavy CH_4 production by a hyperthermophilic methanogen under high-pressure cultivation. *Proceedings of the National Academy of Sciences* 105, 10949–10954. https://doi.org/10.1073/pnas.0712334105

Tivey, M.A., Bradley, A.M., Joyce, T.M., Kadko, D. (2002) Insights into tide-related variability at seafloor hydrothermal vents from time-series temperature measurements. *Earth and Planetary Science Letters* 202, 693–707. https://doi.org/10.1016/S0012-821X(02)00801-4

Truong, C., Bernard, S., Le Pape, P., Morin, G., Baya, C., Merrot, P., Gorlas, A., Guyot, F. (2023) Production of carbon-containing pyrite spherules induced by hyperthermophilic Thermococcales: a biosignature? *Frontiers in Microbiology* 14, 1145781. https://doi.org/10.3389/fmicb.2023.1145781

Truong, C., Bernard, S., Baudin, F., Gorlas, A., Guyot, F. (2024) Carbon-containing pyrite spherules: mineral biosignature in black smokers? *European Journal of Mineralogy* 36, 813–830. https://doi.org/10.5194/ejm-36-813-2024

Geochemical Perspectives Letters

Abiotic syntheses of pyrite: Clues to assess the biogenicity of pyrite spherules

C. Truong, S. Bernard, A. Gorlas, F. Guyot

Supplementary Information

The Supplementary Information includes:

- Methods
- Figures S-1 to S-3
- Supplementary Information References

Methods

Chimney sample from a black smoker at the Trans-Atlantic Geotraverse (TAG)

The natural sample of black smoker described in this study was sampled during the Bicose 2 campaign, operation BIC2-PL01-01, on February 4th 2018 by the Nautile submersible (Cambon, 2018). The chimney was located at 26° 8.223' N - 44° 49.532' W at a depth of 3640 m. The chimney part was placed in a collection box, brought to the surface and directly introduced into anaerobic flask onboard. The sample was stored in an anaerobic flask filled with seawater from the sampling site and the gas phase was replaced by N_2 to limit interaction with O_2. It was stored at 4 °C for 1 year, then the solid phase was vacuum-dried in an anoxic Jacomex™ glove-box under an N_2 atmosphere (<1 ppm O_2). Dry sample was kept at 4 °C in sterile Eppendorf before being analysed in the present study.

Preparation of cell lysates and separation of cellular components

T. kodakarensis KOD1 cultures were prepared as described in Gorlas *et al.* (2018). Cells were grown during 12 h at 85 °C to reach the early stationary phase with final concentrations of 5.10^7 cells mL^{-1}. The cell lysates preparation was conducted in aerobic conditions while the separation of cellular components was carried out in strict anaerobic conditions in an anoxic Jacomex™ glovebox (<10 ppm O_2, Ar atmosphere) (Fig. S-3). The cell lysates were made from 50 mL of *T. kodakarensis* KOD1 culture in a modified Ravot medium (see Gorlas *et al.*, 2018) supplemented with 1g (w/v) elemental sulfur. The remaining elemental sulfur was then removed by sedimentation from the culture for 5 minutes, before recovering the liquid part. The whole culture was centrifuged at 3000 g for 15 min. The supernatant was discarded and the cell pellet was suspended in 5 mL of ultrapure (MilliQ) water, then centrifuged again at 3000 g for 15 min. The supernatant was removed and the cell pellet passed through an ultrasonic bath for 15 min. The cell pellet was then frozen at -20 °C and thawed twice, finally stored at 2 °C until the experiment.

Separation of cellular components was also carried out using 50 mL of *T. kodakarensis* KOD1 culture, which was passed through an ultrasonic bath for 15 min and reintroduced into the glovebox (Fig. S-3). The whole culture was then centrifuged at 3000 g for 15 min directly in the glovebox to separate the supernatant and the intracellular material from the cell envelopes. The liquid part (supernatant + intracellular material) was finally filtrated at 0.2 µm to avoid any envelopes residues. The cell envelopes were resuspended in the synthesis medium before mineralization experiments.

Mineralisation protocol in anoxic conditions

Each synthesis was carried out under strictly anaerobic conditions in an anoxic JacomexTM glove box (<10 ppm O_2, Ar atmosphere). The syntheses were conducted at 85 °C for 96 hr in titanium reaction bombs filled with 10 mL of a Ravot medium traditionally used for Thermococcales growth, however devoided of organic matter (named "Ravot mineral medium"). The Ravot mineral medium contains, per litre of distilled water: 1 g NH_4Cl, 0.2 g $MgCl_2.6H_2O$, 0.1g $CaCl_2.2H_2O$, 0.1 g KCl, 0.83 g, 20g NaCl, 3 g PIPES, 0.001 g resazurin and Na_2S (1.3 mM) to reduce the medium. The pH was adjusted to 7 before autoclaving. After autoclaving, 5 ml of 6 % (w/v) K_2HPO_4 solution and 5 ml of 6 % (w/v) KH_2PO_4 solution were added aseptically. The medium was then supplemented with colloidal sulfur (20 mM) from a solution at 10% (m/v), ferrous iron ($FeSO_4$ 5mM) and the various organic compounds (with the exception of the negative control): the KOD1 lysates, the KOD1 envelopes, yeast extract (1g/L) and tryptone (1g/L), or graphitic carbon (2g/L). In the case of KOD1 intracellular material synthesis, 10 mL of the mixture of supernatant and intracellular material was used directly. Colloidal sulfur (30 g, Sigma-Aldrich, product number 13825) was vigorously mixed in 350 mL distilled water and centrifuged at 3000 g for 5 minutes. The pellet was rinsed 10 times with MilliQ water, resuspended in 10 % final MilliQ water, and filtered through 0.45 µm polycarbonate filters before use. The syntheses were performed in triplicates (graphite, yeast extract + tryptone, negative control) or duplicates (lysates, envelopes and intracellular content). Each synthesis (triplicates and duplicates) were observed by SEM, but we selected one sample of each for the FIB sections, TEM and STXM analyses.

Scanning electron microscopy coupled with energy dispersive X-ray spectroscopy

Minerals were investigated using Scanning Electron Microscopy (SEM) coupled with Energy-Dispersive X-ray Spectroscopy (EDXS). Samples were dried in an anoxic Jacomex^{TM} glove box (<10 ppm O_2, Ar atmosphere). Sample dry powders (natural chimney and experimental syntheses) were deposited on a carbon tape and carbon-metallised. SEM-EDXS data were collected at IMPMC, MNHN Electron Microscopy and Microanalysis Technical Platform, with a GEMINI ZEISS^{TM} Ultra55 Field Emission Gun Scanning Electron Microscope equipped with two Bruker™ XFlash silicon drift detectors in antagonist positions for EDXS. Both images and EDXS data were collected using an acceleration voltage of 15 kV at a working distance of 12 mm and 300 pA probe current.

Sample preparation by focused ion beam

Focused ion beam (FIB) foils (20µm * 5µm * 100nm) were extracted from a pyrite of TAG sample and from pyrite synthetized in presence of KOD1 lysates, KOD1 envelopes, KOD1 YE + tryptone or graphitic carbon syntheses, never exposed to high acceleration voltage using a FEI Strata DB 235 (IEMN, Lille, France). Milling at low gallium ion currents allowed minimizing common artefacts including local gallium implantation, mixing of components, redeposition of the sputtered material on the sample surface and significant changes in the speciation of carbon-based polymers (Bernard *et al.*, 2009; Schiffbauer and Xiao, 2009).

Transmission electron microscopy

FIB sections of the samples were analysed using a JEOL JEM-2100F at IMPMC, equipped with a field emission gun (FEG) operating at 200kV. Identification of minerals was done by selected-area electron diffraction (SAED) and energy-dispersive X-ray spectroscopy (EDXS) in Scanning TEM (STEM) mode.

Scanning transmission X-ray microscopy

Scanning transmission X-ray microscopy (STXM) analyses were performed on FIB sections to document the carbon speciation of the organic compounds trapped within the pyrite using the HERMES STXM beamline at the synchrotron SOLEIL (Saint-Aubin, France - Belkhou *et al.*, 2015; Swaraj *et al.*, 2017). We did the energy calibration using the well-resolved 3p Rydberg peak of gaseous CO_2 at 294.96eV for the C K-edge. X-ray absorption near edge structure (XANES) hypercube data (stacks) were collected with a spatial resolution of 100 nm at energy increments of 0.1eV over the carbon (270–340eV) absorption range with a dwell time of less than 1ms per pixel to prevent irradiation damage (Wang *et al.*, 2009). Stack alignments and extraction of XANES spectra were done using the using the Hyperspy python-based package (De La Peña *et al.*, 2018). Data was normalized using the QUANTORXS freeware (Le Guillou *et al.*, 2018). A spectral parameter ($[C]_{STXM}$) was extracted from spectra collected at the C-K edge to provide a non-calibrated estimation of the concentration in C. The $[C]_{STXM}$ values reported here correspond to the ratio between the carbon quantity (estimated from the area of the spectra from 280 to 291.5 eV after subtraction of a power law fitting the pre-edge region - see Le Guillou *et al.*, 2018 for details) and the absorption at 280 eV (before substraction of the power law). By construction, the $[C]_{STXM}$ values are proportional to the atomic concentration of carbon in the pyrites, but given that no calibration was conducted, these values only provide qualitative information rather than absolute concentrations.

Supplementary Figures

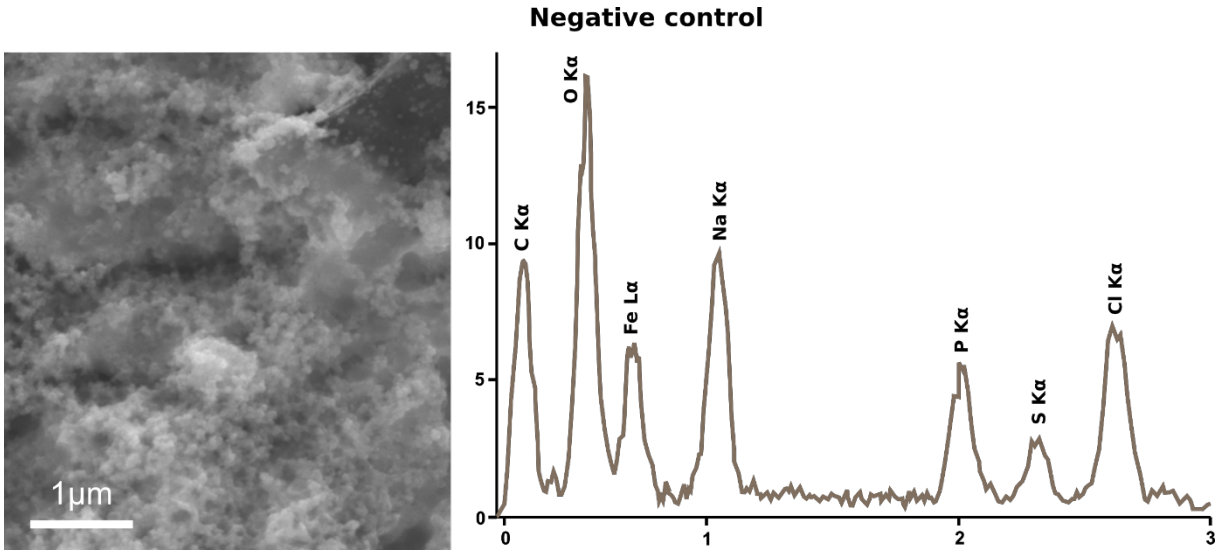

Figure S-1 EDXS spectrum of the material observed in the negative control (in absence of organic material).

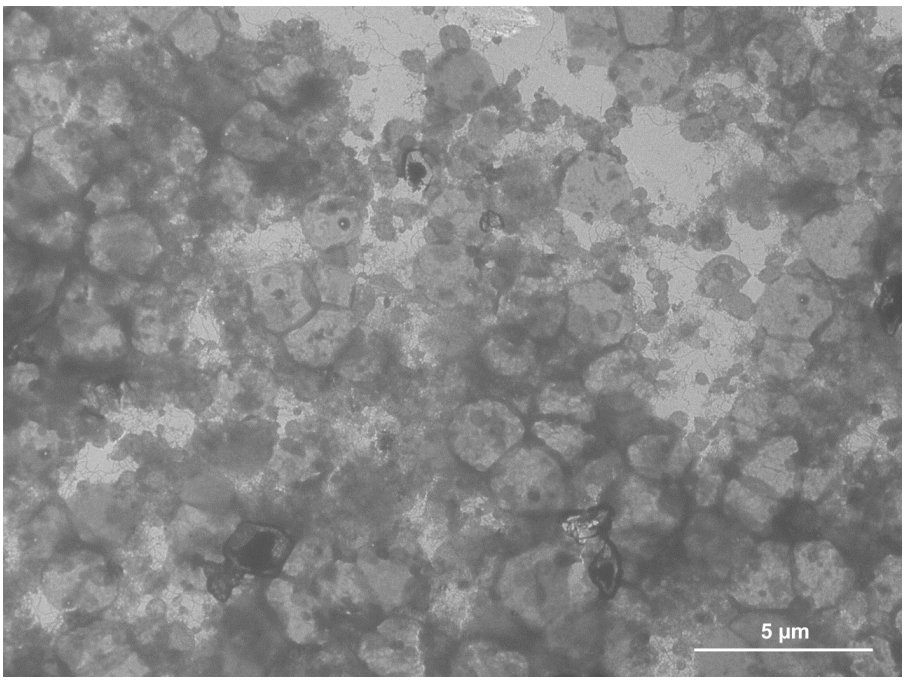

Figure S-2 TEM observation of the cell envelopes after the separation protocol. The envelopes appear translucent (emptied of their intracellular contents) while the overall integrity of the envelopes is preserved. Numerous flagella and vesicles are also visible.

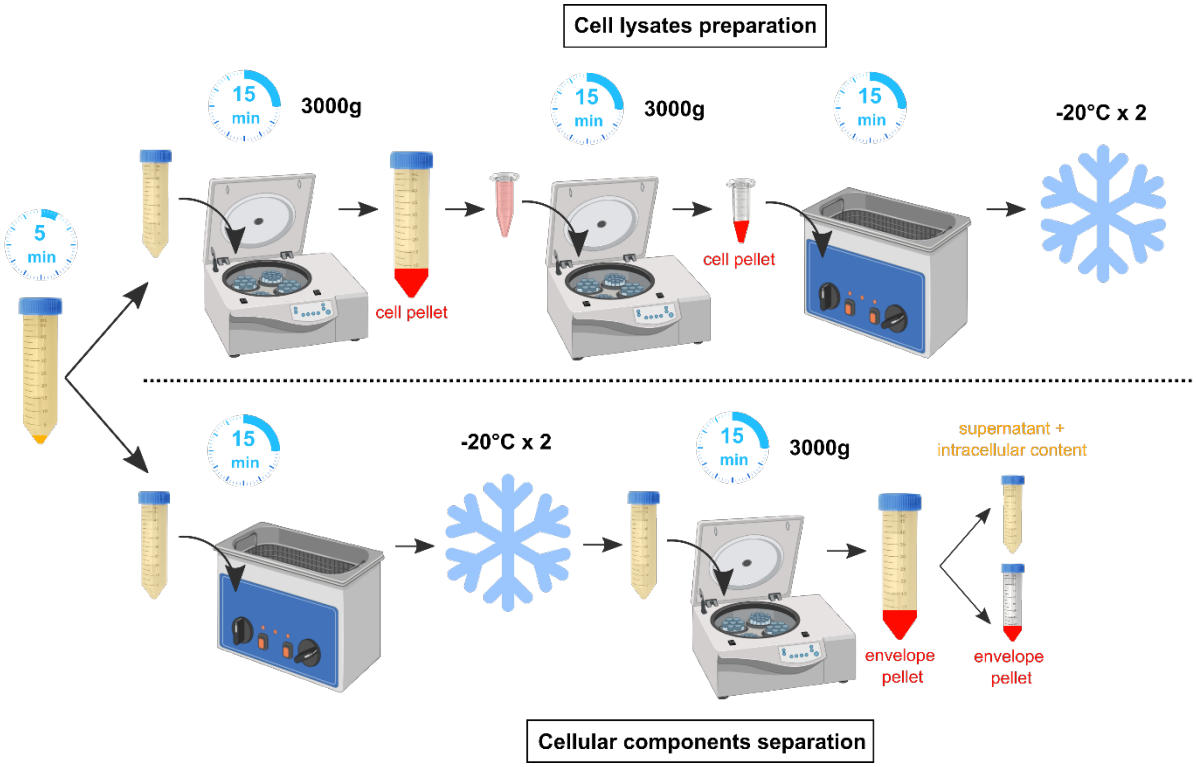

Figure S-3 Diagram of the cell lysate preparation and cell components separation protocol.

Supplementary Information References

Belkhou, R., Stanescu, S., Swaraj, S., Besson, A., Ledoux, M., Hajlaoui, M., Dalle, D. (2015) HERMES: a soft X-ray beamline dedicated to X-ray microscopy. *Journal of Synchrotron Radiation* 22, 968–979. https://doi.org/10.1107/S1600577515007778

Bernard, S., Benzerara, K., Beyssac, O., Brown, G.E., Grauvogel Stamm, L., Duringer, P. (2009) Ultrastructural and chemical study of modern and fossil sporoderms by Scanning Transmission X-ray Microscopy (STXM). *Review of Palaeobotany and Palynology* 156, 248–261. https://doi.org/10.1016/j.revpalbo.2008.09.002

Blanc, P., Lassin, A., Piantone, P., Azaroual, M., Jacquemet, N., Fabbri, A., Gaucher, E.C. (2012) Thermoddem: A geochemical database focused on low temperature water/rock interactions and waste materials. *Applied Geochemistry* 27, 2107–2116. https://doi.org/10.1016/j.apgeochem.2012.06.002

Cambon, M.-A. (2018) BICOSE 2 cruise, RV Pourquoi pas? https://doi.org/10.17600/18000004

De la Peña, F., Ostasevicius, T., Fauske, V.T., Burdet, P., Prestat, E., Jokubauskas, P., Nord, M., MacArthur, K.E., Sarahan, M., Johnstone, D.N., Taillon, J., Eljarrat, A., Migunov, V., Caron, J., Furnival, T., Mazzucco, S., Aarholt, T., Walls, M., Slater, T., Winkler, F., Martineau, B., Donval, G., McLeod, R., Hoglund, E.R., Alxneit, I., Hjorth, I., Henninen, T., Zagonel, L.F., Garmannslund, A. (2018) hyperspy/hyperspy v1.4.1. Zenodo. https://doi.org/10.5281/zenodo.1469364

Gorlas, A., Jacquemot, P., Guigner, J.-M., Gill, S., Forterre, P., Guyot, F. (2018) Greigite nanocrystals produced by hyperthermophilic archaea of Thermococcales order. *PLoS One* 13, e0201549. https://doi.org/10.1371/journal.pone.0201549

Le Guillou, C., Bernard, S., De la Peña, F., Le Brech, Y. (2018) XANES-Based Quantification of Carbon Functional Group Concentrations. *Analytical Chemistry* 90, 8379–8386. https://doi.org/10.1021/acs.analchem.8b00689

Schiffbauer, J., Xiao, S. (2009) Novel application of focused ion beam electron microscopy (FIB-EM) in preparation and analysis of microfossil ultrastructures: A new view of complexity in early Eukaryotic organisms. *Palaios* 24, 616–626. https://doi.org/10.2110/palo.2009.p09-003r

Swaraj, S., Stanescu, S., Rioult, M., Besson, A., Hitchcock, A.P. (2017) Performance of the HERMES beamline at the carbon K-edge. *Journal of Physics: Conference Series* 849, 012046. https://doi.org/10.1088/1742-6596/849/1/012046

Wang, J., Morin, C., Li, L., Hitchcock, A.P., Scholl, A., Doran, A. (2009) Radiation damage in soft X-ray microscopy. *Journal of Electron Spectroscopy and Related Phenomena* 170, 25–36. https://doi.org/10.1016/j.elspec.2008.01.002